Robust localization using 3D NDT scan matching with experimentally determined uncertainty and road marker matching

Conference Paper · June 2017

DOI: 10.1109/IVS.2017.7995900

5 authors, including:

Naoki Akai
Nagoya University
76 PUBLICATIONS **537** CITATIONS
SEE PROFILE

Y. Morales
Standard Cognition
98 PUBLICATIONS **1,350** CITATIONS
SEE PROFILE

Yuki Yoshihara
Nagoya University
35 PUBLICATIONS **229** CITATIONS
SEE PROFILE

Yoshiki Ninomiya
Nagoya University
82 PUBLICATIONS **1,940** CITATIONS
SEE PROFILE

Robust Localization Using 3D NDT Scan Matching with Experimentally Determined Uncertainty and Road Marker Matching

Naoki Akai[1], Luis Yoichi Morales[1], Eijiro Takeuchi[2], Yuki Yoshihara[1], and Yoshiki Ninomiya[1]

***Abstract*— In this paper, we present a localization approach that is based on a point-cloud matching method (normal distribution transform "NDT") and road-marker matching based on the light detection and ranging intensity. Point-cloud map-based localization methods enable autonomous vehicles to accurately estimate their own positions. However, accurate localization and "matching error" estimations cannot be performed when the appearance of the environment changes, and this is common in rural environments. To cope with these inaccuracies, in this work, we propose to estimate the error of NDT scan matching beforehand (off-line). Then, as the vehicle navigates in the environment, the appropriate uncertainty is assigned to the scan matching. 3D NDT scan matching utilizes the uncertainty information that is estimated off-line, and is combined with a road-marker matching approach using a particle-filtering algorithm. As a result, accurate localization can be performed in areas in which 3D NDT failed. In addition, the uncertainty of the localization is reduced. Experimental results show the performance of the proposed method.**

I. Introduction

Localization is a fundamental technique for autonomous driving. Accurate localization can be utilized to improve the performance of path tracking and planning and perception functions that are required for advanced autonomous driving. This paper proposes a robust and accurate localization method using multilayer light detection and ranging (LiDAR). In this study, we use three-dimensional (3D) point-cloud and road-marker maps built by Mobile Mapping System (MMS) [1].

In road environments, there are different objects that can be used as landmarks, such as road markers, signs, curbs, and poles. Localization methods using these objects have been previously proposed [2], [3], [4], [5], [6]. These methods can perform accurate localization in areas where there is a sufficient number of landmarks. However, public roads include areas without those landmarks, e.g., residential streets and mountainous forested roads. In such areas, other types of localization are required to perform advanced autonomous driving.

Levinson *et al.* proposed a map-based localization method in [7]. The map that was used was built using LiDAR, which is installed on the vehicle. This method can be used in various areas because it does not require specific landmarks. A similar approach was proposed in [8]. However, map-based localization methods cannot perform robust localization for environments whose appearance changes. Unfortunately, the appearances of public roads are prone to change because of their proximity to forests and crop fields. To cope with this problem, a localization method using tree and dynamic obstacle detection, called change detection, was proposed [9]. However, object recognition is not trivial and change detection remains an open problem.

The normal distribution transform (NDT) can cope with slight environmental changes because an environmental map is represented by a set of normal distributions [10], [11]. In particular, the robustness of scan matching using NDT is higher than that of point-to-point-based iterative closest

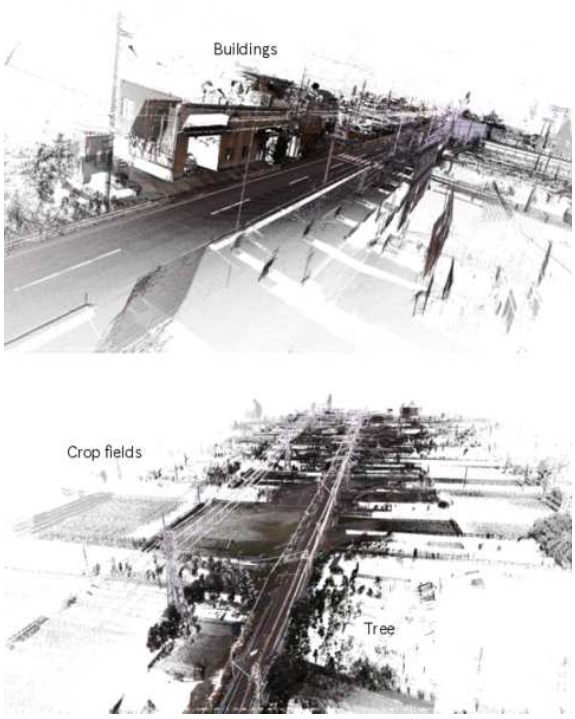

Fig. 1. 3D point-cloud map built by MMS. The convergence performance of scan matching depends on the shape of the environment. Scan matching converges in the environment like the one on the top figure because buildings are good features. However, the convergence performance is reduced in the environment, such as with the bottom figure because there are few good features. In this work, we propose to estimate the error of the scan matching in each area beforehand (off-line). Then, as the vehicle navigates in the environment, the appropriate uncertainty is assigned to the scan matching.

*This work was supported by the Center of Innovation Program (Nagoya-COI) from the Japan Science and Technology Agency.

[1]Naoki Akai, Luis Yoichi Morales, Yuki Yoshihara, and Yoshiki Ninomiya are with the Institute of Innovation for Future Society (MIRAI), Nagoya University, Nagoya 464-8603, Japan {akai, morales_yoichi, y-yuki, ninomiya}@coi.nagoya-u.ac.jp

[2]Eijiro Takeuchi is with the Graduate School of Information Science, Nagoya University, Nagoya 464-8603, Japan e_takeuchi@is.nagoya-u.ac.jp

point (ICP) scan matching [12]. However, NDT sometimes falls into a local minimum when the accuracy of the initial pose is low. It is reported that the error of NDT when scan matching fails is larger than that of ICP scan matching [12]. In addition, the convergence performance of NDT depends on the appearance of the environment, and the localization accuracy decreases in the case where there are differences between the environment and map.

In this work, we estimate the error of 3D NDT scan matching in each area beforehand (off-line). As shown in Fig. 1, the convergence performance of the 3D NDT depends on environmental conditions. By performing off-line experiments, the appropriate uncertainty can be assigned to the scan matching as the vehicle navigates in the environment. 3D NDT scan matching utilizes the uncertainty information that is estimated off-line, and is combined with a road-marker matching approach using the particle filtering (PF) algorithm [13]. As a result, accurate localization can be performed in areas where the 3D NDT failed. In addition, the uncertainty of the localization is reduced.

The contributions of this paper are as follows.

- The uncertainty of NDT scan matching is well estimated by performing a pre-experiment.
- The proposed localization method robustly estimates a vehicle pose even though NDT may fail.
- Robust and accurate localization is achieved in public roads using maps that were built in different seasons (map building was done in summer and localization experiments were conducted in winter).

The rest of this paper is composed as follows. In Section II, we describe related works. In Section III, we present details about NDT scan matching, and we investigate its convergence performance by performing a pre-experiment. Then, we present details of the proposed localization method in Section IV, while we describe experiments including comparison in Section V. In Section VI, we conclude the paper.

II. Related Works

In [14], the authors propose a method that is similar to our proposed method. This method uses 3D point-cloud and road-marker matching methods. A 3D point-cloud map is divided according to height, and ICP scan matching is performed in each layer. In their proposal, three ICP results are obtained, and these results are combined using the weighted average, where the weight of the estimated results obtained from each layer are determined by considering the error of the ICP. In addition, the road-marker matching result is used to compensate for lateral error. Although our proposal is similar to this method, we newly added an uncertainty estimation of the 3D point-cloud map-based localization, i.e., 3D NDT. This estimate increases the robustness to failures in the NDT.

Several methods have been proposed to estimate the uncertainty of the scan-matching algorithm. Bengtsson *et al.* proposed a method that uses the Hessian matrix of the error function [15]. However, it has a problem in that an incorrect probabilistic distribution will be generated when exact correspondences between scan and target points are not obtained. The method proposed by Censi can cope with this problem by using not only the Hessian matrix but also partial differential regarding scan points [16]. However, it is reported that the computation process of the method will be redundant. Olson proposed a brute force method that searches discretized space to determine the probabilistic distribution of the scan matching result [17]. Olson used several techniques to reduce the computation time, e.g., using a lookup table and GPU. However, the computational cost is still high. In addition, a wide range of should be searched to accurately determine the probabilistic distribution, and it also requires significant computational resources.

NDT-based localization has been extensively studied by Lilienthal *et al*. They proposed NDT-based Monte Carlo Localization (MCL), and reported that the accuracy of NDT-based MCL is higher than that of grid-based MCL [18]. Although the uncertainty of the localization result can be obtained from MCL, significant computation resources would be required for application to 3D localization. They also proposed an extended method that uses dual time-scale ND maps to improve the robustness to environmental change [19]. Highly accurate localization was achieved in a dynamic environment using this method. However, the estimated result would not converge if localization fails because the method builds its ND map on-line, and on-line map building is expected to fail.

In our approach, we investigate the convergence performance of NDT scan matching by performing a pre-experiment, and we utilized this result to determine the uncertainty of NDT. Even though this method requires a pre-experiment, the uncertainty of NDT can be well estimated.

III. NDT Scan Matching and Investigation of Convergence Performance

A. Experimental Platform

Fig. 2 shows an experimental platform used in this study. We used Ubuntu and the Robot Operating System (ROS) as the development environment. This vehicle installs HDL-64E as LiDAR, and an Inertial Navigation System (INS) that includes a wheel encoder and a gyro sensor. The two-dimensional (2D) pose, which includes the position, x and y, and yaw angle, θ, is updated by the INS. Because the wheel encoder is attached to the right rear wheel, the motion model of the vehicle is denoted as follows:

$$\begin{pmatrix} x_t \\ y_t \\ \theta_t \end{pmatrix} = \begin{pmatrix} x_{t-1} \\ y_{t-1} \\ \theta_{t-1} \end{pmatrix} + \begin{pmatrix} \Delta d_t \cos\theta_{t-1} \\ \Delta d_t \sin\theta_{t-1} \\ \Delta\theta_t \end{pmatrix}, \quad (1)$$

where $\mathbf{u}_t = (\Delta d_t, \Delta\theta_t)^T$ denotes moving amount of translation and rotation measured by INS from $t-1$ to t. Note that this pose represents the center of the rear wheel axle.

B. NDT Scan Matching

A 3D ND map, which is represented as a voxel map, was built beforehand from a 3D point cloud. Let P_i =

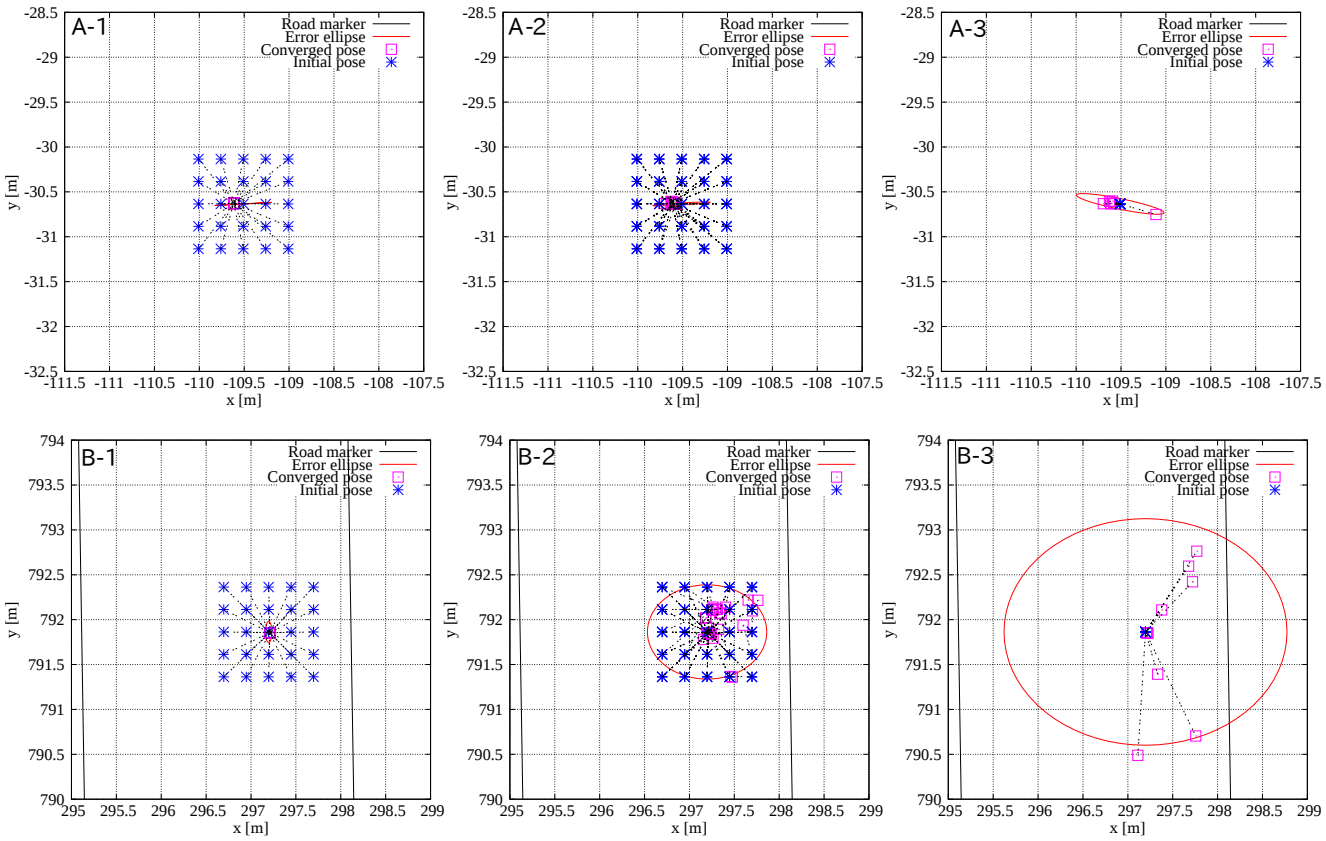

Fig. 4. Investigation results of convergence performance of NDT. Top and bottom results were obtained at areas A and B shown in Fig. 3. After NDT was converged, we executed NDT again from different initial poses. Blue and purple dots represent the initial and converged poses, respectively. The corresponding initial and converged poses are connected with a dashed line. Red ellipses represent a region where the existing probability of the converged pose exceeds 99 %. We conducted each investigation using the following conditions, which represent differences from the first converged pose: (left) $-0.5 \leq x, y \leq 0.5$, every 0.25 m, (middle) $-0.5 \leq x, y \leq 0.5$, $-2 \leq \theta \leq 2$, every 0.25 m and 2 deg, (right)$-5 \leq \theta \leq 5$ every 1 deg.

Fig. 2. Experimental platform.

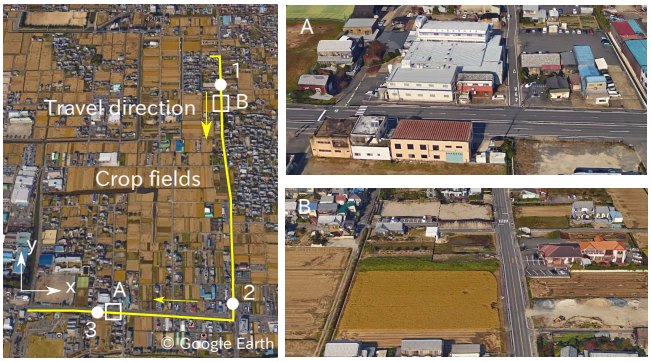

Fig. 3. Bird's-eye view of the experimental environment.

$(\mathbf{p}_{i,1}, \mathbf{p}_{i,2}, ..., \mathbf{p}_{i,N_i})$ be 3D points included in voxel i. Voxel i contains a 3D mean point, $\mathbf{p}_i^m$, and the covariance of the points, Σ_i.

In the localization phase, the initial pose used for the scan matching is determined by the motion model. The measured point cloud from HDL-64E is filtered using a voxel grid (VG) filter, which reduces the number of points. The voxel size of both the ND map and VG filter was set to 1 m. We performed scan matching using the filtered points, $Q = (\mathbf{q}_1, \mathbf{q}_2, ..., \mathbf{q}_M)$. A 3D pose, $\mathbf{x}$, which includes positions x, y, and z, as well as roll, pitch, and yaw angles, ψ, ϕ, and θ, respectively, was estimated by maximizing the following cost function, $J(\mathbf{x})$:

$$J(\mathbf{x}) = \sum_{i=1}^{M} \exp\left\{-\frac{1}{2}(\mathbf{p}_i^m - \mathbf{q}_i^{'})^T \Sigma_i^{-1} (\mathbf{p}_i^m - \mathbf{q}_i^{'})\right\}, \quad (2)$$

$$\mathbf{q}_i^{'} = R\mathbf{q}_i + \mathbf{t}, \quad (3)$$

where R and $\mathbf{t}$ respectively denote the rotation matrix and a translation vector related to the vehicle pose, and $\mathbf{p}_i^m$ and Σ_i

respectively denote the mean point and covariance included in voxel i, which corresponds to $\mathbf{q}_i^{'}$. We used the Gauss-Newton method to maximize the cost function. Finally, we obtained the estimated pose using NDT, $\hat{\mathbf{x}}$. The processing time of the implemented NDT scan matching is less than 0.1 s. More details can be found in [20].

C. Convergence Performance of NDT

We acquired log data using the vehicle, and conducted an off-line experiment to investigate the convergence performance of NDT. Fig. 3 shows a bird's-eye view of the experimental environment. The 3D point-cloud and road-marker maps of the environment were built by AISAN TECHNOLOGY Co. Ltd. during the summer of 2016. Data logging was conducted in December, 2016 according to the yellow line. This suggests that there are some differences between the map and environment, which are due to seasonal change because of the abundance of crop fields.

In this investigation, we first applied NDT scan matching in each position in which readings of HDL-64E were updated (the measurement period is 10 Hz). After NDT converged, we executed NDT again from different initial poses that were slightly different from the first converged pose. Note that we changed the elements of only the 2D pose. The results are shown in the top and bottom figures in Fig. 4. These results were obtained in areas A and B, as shown in Fig. 3, respectively. The left figures show the result when only x and y values were changed from the first converged pose. The convergence performance is good in both areas. The middle figures show the result obtained when x, y, and θ values were changed. The θ value was changed from -2 deg to 2 deg in increments of 2 deg. The convergence performance slightly decreased in both cases. Finally, the right figures show the result when the θ value was significantly changed. The θ value was changed from -5 deg to 5 deg in increments of 1 deg. It is evident that the accuracy of the heading direction of the initial pose significantly affects the convergence performance, and the convergence performance differs for each area.

Figs. 5 and 6 show depth maps and the histograms obtained in areas A and B. An open space can be confirmed on both side of area B because crop fields are close. In contrast, there are objects on both sides of area A. These results strongly suggest that the convergence performance depends on the environmental conditions of each area.

The convergence performance depends on the initial pose. There may be a large uncertainty in the case where the investigation involves the use of an initial pose that is significantly different from the first converged pose. Therefore, we empirically considered only errors that would appear in the actual localization phase, and we investigated the convergence performance. Finally, we used the result that was obtained when θ value was only changed from -5 deg to 5 deg, and we computed the covariance matrix, $\mathrm{cov}(\hat{\mathbf{x}})$, from the result. Fig. 7 shows the trace of the covariance matrix according to the path.

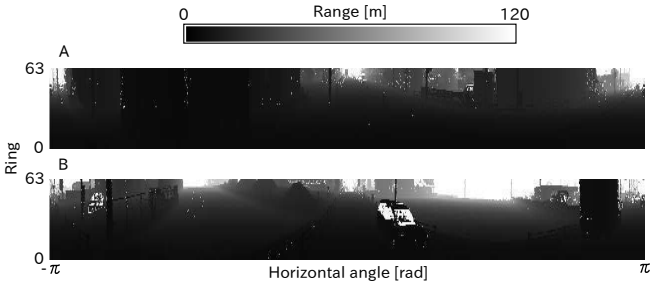

Fig. 5. Depth map created from HDL-64E at areas A and B shown in Fig. 3.

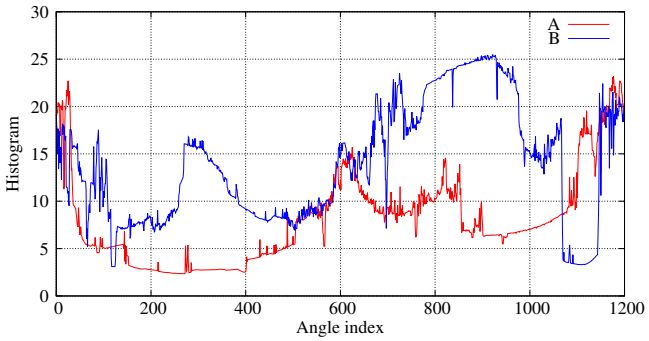

Fig. 6. Histogram of the depth map shown in Fig. 5. The maximum range (120 m) of each pixel is normalized to one, and the values of each column are added. The angle index 600 is the front direction of HDL-64E. The histogram of depth map B has a greater depth and A as it is not surrounded by buildings.

IV. Localization Using 3D Point Cloud and Road Marker Maps

This section provides details of the road-marker matching and the proposed localization method utilizing a particle filter to combine dead reckoning, NDT, and road-marker matching.

A. Road-Marker Map and Detection

A road-marker map is represented as a 2D likelihood map. Fig. 8 shows an example of the road-marker map. The grid size of the map was set to 0.2 m.

The road marker is detected from the readings of HDL-64E. Because road markers are drawn on road surfaces, road surface points are first detected. To detect ground points, we created a depth map of the readings and computed a normal vector of each point. Details of the process can be found in [21]. Points with a normal vector that value of z-direction element (coordinates of HDL-64E) exceeds 0.8 are detected as road surface points. In addition, we clipped these points to remove points that are obviously far from the road surface.

HDL-64E can measure values of reflection intensity that are normalized within the range 0-255. Road markers are detected as reflectors, and their reflection intensities are therefore large. We set an intensity threshold value of 170,

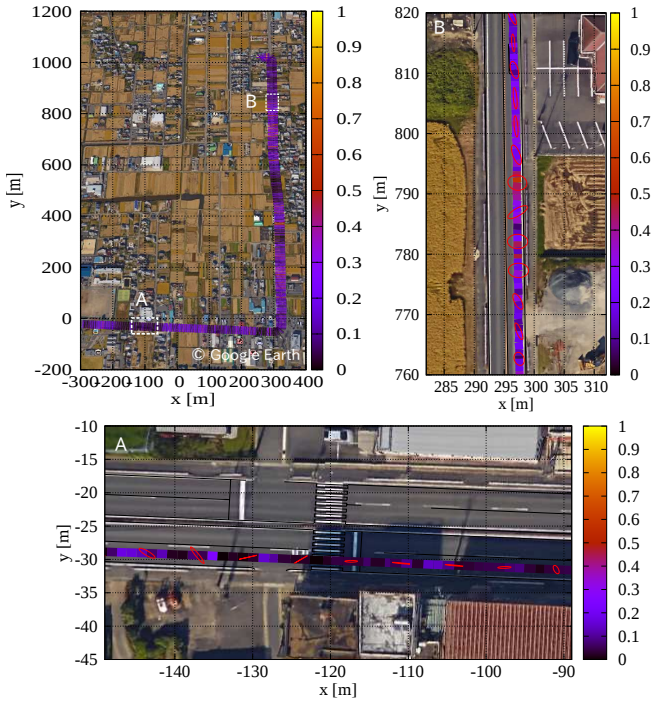

Fig. 7. Trace of the covariance matrix computed from the investigation of convergence performance of NDT. Red ellipses depict an error ellipse determined from the covariance matrix.

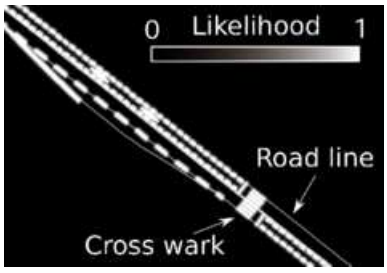

Fig. 8. Likelihood field of road marker.

so road surface points with reflection intensities that exceed the threshold are detected as road marker points, $Z = (\mathbf{z}_1, \mathbf{z}_2, ..., \mathbf{z}_K)$. Fig. 9 shows an example of the image of the road-marker detection method.

B. Proposed Localization System

We used the PF algorithm to implement the proposed localization system. Although NDT scan matching estimates the 3D pose, this PF estimates a 2D pose. Particles are updated by the motion model shown in Eq. (1). The observation model of road marker, $p(Z_t|\mathbf{x}_t)$, is denoted as follows:

$$p(Z_t|\mathbf{x}_t) \propto \prod_{i=1}^{K} \exp\left\{-\frac{1}{2}(\mathbf{z}_i^{'} - \boldsymbol{\mu}_i)^T \Sigma_l^{-1} (\mathbf{z}_i^{'} - \boldsymbol{\mu}_i)\right\}, \quad (4)$$

$$\mathbf{z}_i^{'} = R_j \mathbf{z}_i + \mathbf{t}_j, \quad (5)$$

where R_j and $\mathbf{t}_j$ denote the rotation matrix and the translation vector computed from the j-th particle, respectively, and

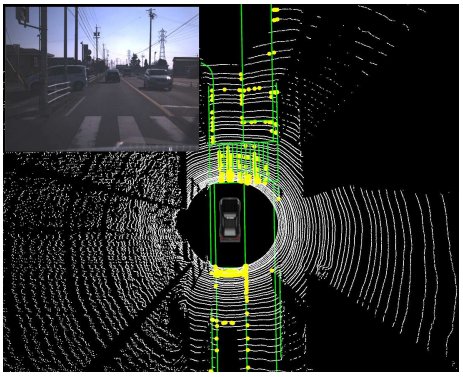

Fig. 9. An example of road-marker-point detection and camera image. White and yellow dots depict points that are detected as road-surface and road-marker points. Green lines represent the road-marker map.

$\Sigma_l = \mathrm{diag}(\sigma_l^2, \sigma_l^2)$ and $\boldsymbol{\mu}_i$ respectively denote the covariance matrix of LiDAR readings and the grid position of the road-marker map corresponding to $\mathbf{z}_i^{'}$. We set σ_l to 0.2 by considering the grid size.

In the proposed method, NDT scan matching is running in parallel. The PF system receives the estimated pose by NDT, $\hat{\mathbf{x}}$. The result from NDT has the covariance matrix, $\mathrm{cov}(\hat{\mathbf{x}})$, that was computed in each position in the pre-experiment. We then calculated the likelihood of the particles using the following observation model:

$$p(Z_t|\mathbf{x}_t)\mathcal{N}(\mathbf{x}_t; \hat{\mathbf{x}},\ \mathrm{cov}(\hat{\mathbf{x}})), \quad (6)$$

where $\mathcal{N}(\mathbf{x}_t; \hat{\mathbf{x}},\ \mathrm{cov}(\hat{\mathbf{x}}))$ denotes the Gaussian distribution, which represents the uncertainty of NDT.

In order to avoid the incorrect convergence of particles, resampling should be done only in the case in which there is a bias in the likelihood. In this study, we used the effective sample size (ESS) [22], and resampling is done when the following condition is satisfied:

$$\frac{1}{\sum_{i=1}^{N_p}(w_i^2)} < 0.9, \quad (7)$$

where w_i and N_p denote the normalized likelihood of the i-th particle and number of particles, respectively. We set the number of particles to 1000. In addition, 5 % of random particles are mixed when resampling is performed.

V. Experiment

A. Condition

We conducted experiments in the environment shown in Fig. 3. The maps that were used in the pre-experiment were also used for the evaluation. We conducted an autonomous driving demonstration in December, 2016, and we took logs of the demonstration [1]. We performed an evaluation was using the log data generated during autonomous driving experiments. The navigation speed of the vehicle was approximately 50 km/h.

[1]Videos of the autonomous driving demonstration can be found at `https://youtu.be/epMaPSxyCDI`

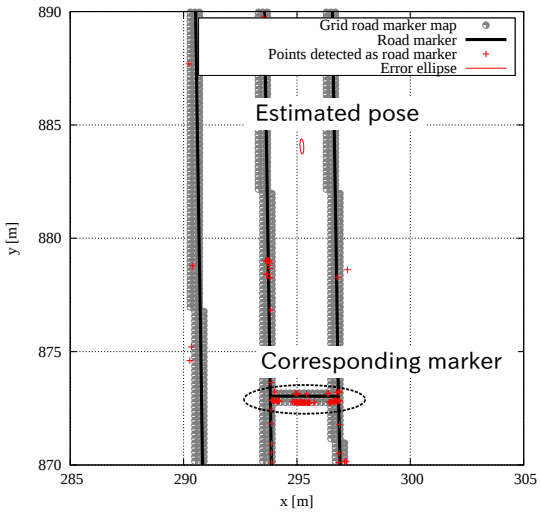

Fig. 10. Evaluation scheme for localization accuracy. Points detected as road markers are plotted from the estimated pose. Then, we manually measured the distance from the points to the corresponding marker.

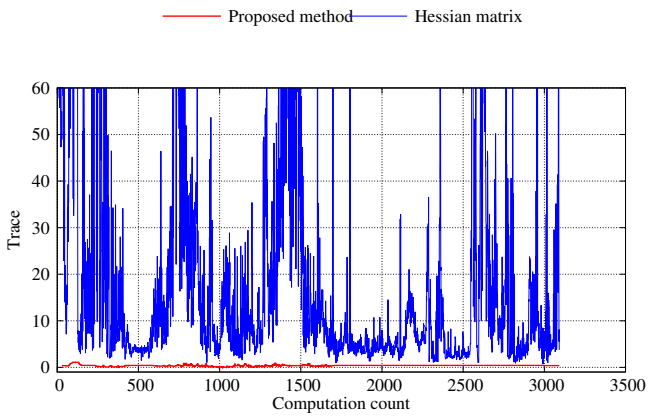

Fig. 12. Trace of the covariance matrix computed from the proposed and Hessian matrix-based methods. Note that the top side of the figure is omitted to clearly display the comparison result.

B. Evaluation and Comparison

We evaluated the localization accuracy using road markers, and Fig. 10 shows the evaluation scheme. The points that were detected as road markers are plotted from the estimated pose. Then, we manually measured the distance from the points and corresponding marker. In the experimental environment, there are three stop lines tha are depicted as white dots in Fig. 3. The longitudinal and lateral errors were measured from the points. We also discussed the performance of the uncertainty estimation of the proposed method based on the results of the accuracy evaluation.

We compared three different approaches.

- The proposed approach utilizing NDT-INS with the pre-computed covariance matrix, and the road marker.
- NDT-INS with the covariance matrix computed from the Hessian matrix (explained in the following subsection) and road marker.
- NDT-INS.

Application of Hessian matrix to determine NDT uncertainty: For the comparison, we implemented another combination method that uses the Hessian matrix to determine the uncertainty of the NDT estimation. This method also provides a covariance matrix of the estimated pose, $\mathrm{cov}(\hat{\mathbf{x}})$, as follows:

$$\mathrm{cov}(\hat{\mathbf{x}}) = \sigma^2 \left(\frac{\partial^2}{\partial \mathbf{x}^2} J(\hat{\mathbf{x}}) \right)^{-1}, \tag{8}$$

where σ^2 denotes the scale of the covariance, and is called the noise level [23]. In this study, we set this value as $\sigma^2 = 2\varepsilon/(M-3)$, which was used in [15], where ε is a summation of errors between corresponding points computed in the scan-matching algorithm. We used the summation of the Mahalanobis distance as follows:

$$\varepsilon = \frac{1}{2M} \sum_{i=1}^{M} (\mathbf{p}_i^m - \mathbf{q}_i^{'})^T \Sigma_i^{-1} (\mathbf{p}_i^m - \mathbf{q}_i^{'}), \tag{9}$$

where the rotation matrix and translation vector used in $\mathbf{q}^{'}$ are computed from $\hat{\mathbf{x}}$.

C. Results

We conducted the experiments four times. Table I shows the longitudinal and lateral errors for each method. The averages of the longitudinal and lateral errors of the proposed method were lowest. In addition, the longitudinal error of the proposed method did not exceed 1 m, even though the error of other methods exceeded 1 m. This result shows that the proposed method enables the vehicle to accurately recognize its own position. Furthermore, for each experiment, Fig. 11 shows trajectories for four iterations. The trajectories of the PF-based methods are smoother than that of NDT.

Fig. 12 shows a comparison of the results for the proposed and Hessian matrix-based methods. This figure shows a trace of the covariance matrix, $\mathrm{Tr}(\mathrm{cov}(\hat{\mathbf{x}}))$, which is computed from each method. It is clear that the Hessian matrix-based method always estimates large uncertainties. As a result, this method cannot perform accurate localization even though NDT worked well. Although the scale of the uncertainty can be controlled by adjusting the noise level, this parameter should be well tuned. Even though the proposed method requires a pre-experiment, it does not require any parametric adjustments.

Finally, Fig. 13 shows the validation results of the uncertainty estimation performance obtained using the proposed method. The estimated trajectories and error ellipses of the proposed, Hessian matrix-based, and NDT only methods are depicted in red, sky blue, and blue, respectively. Each error ellipse represents a region where the existing probability exceeds 99 %, and the ellipse of the proposed method is computed from the distribution of the particles. The centroid of the error ellipse is the estimated pose. The points that were detected as road markers are also depicted in the same color as that of the estimated pose. As can be seen from both figures, the estimated pose obtained by NDT only is slightly

TABLE I

LONGITUDINAL AND LATERAL ERRORS NEARBY STOP LINES.

	Proposed method		Hessian		NDT only	
Experiment number-Stop line number	Longitudinal [m]	Lateral [m]	Longitudinal [m]	Lateral [m]	Longitudinal [m]	Lateral [m]
1-1	0.10	0.03	0.39	0.11	0.10	0.15
1-2	0.10	0.04	0.18	0.10	0.17	0.02
1-3	0.05	0.08	1.67	0.08	1.73	0.05
2-1	0.24	0.09	2.40	0.09	0.81	0.10
2-2	0.01	0.08	0.10	0.07	0.31	0.18
2-3	0.07	0.05	0.11	0.06	0.28	0.06
3-1	0.23	0.05	1.58	0.08	0.53	0.14
3-2	0.23	0.12	2.68	0.15	0.65	0.13
3-3	0.10	0.05	0.39	0.07	0.75	0.04
4-1	0.32	0.11	0.41	0.08	1.17	0.17
4-2	0.52	0.11	3.37	0.09	0.37	0.10
4-3	0.36	0.04	2.60	0.04	0.29	0.05
Average	0.19	0.07	1.32	0.09	0.60	0.10
Standard deviation	0.15	0.03	1.20	0.03	0.47	0.05
Minimum	0.01	0.03	0.10	0.04	0.10	0.02
Maximum	0.52	0.12	3.37	0.15	1.73	0.18

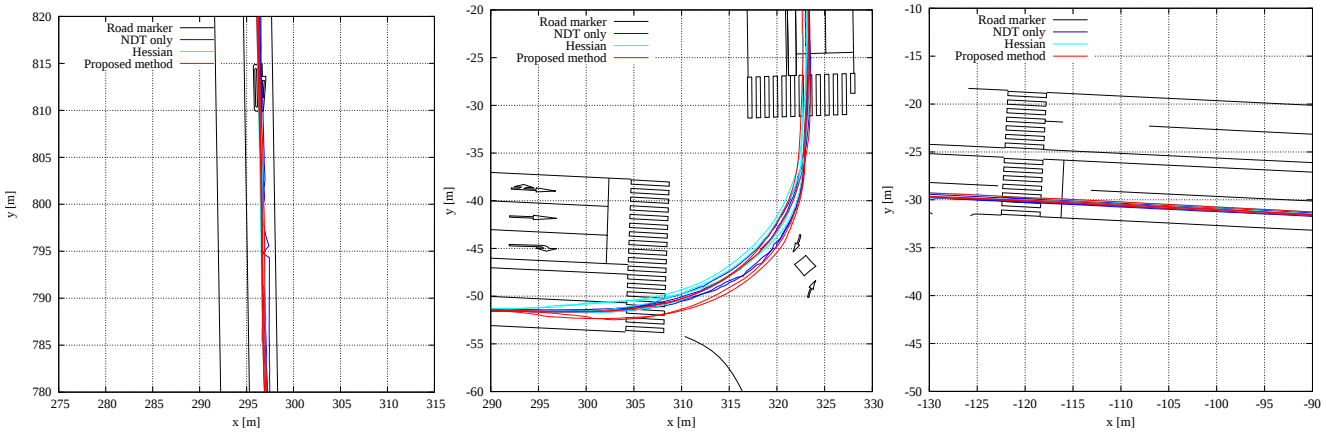

Fig. 11. Trajectories of four times experiments of each method.

different from the ground truth because the road markers are not matched well. However, the errors may be covered by the uncertainty that is determined beforehand (we computed the blue ellipses using the results of the pre-experiment detailed in Section III). Although the uncertainty computed from the Hessian matrix could also cover the error, its region was relatively large compared to the pre-determined region. Note that the error ellipse computed from the Hessian matrix is drawn in the bottom figure, but it is not shown because the range of the ellipse is very large. These results showed that the uncertainty of NDT was well estimated by the proposed method. In addition, the uncertainty of the proposed localization method could be reduced from that of NDT.

VI. CONCLUSION AND FUTURE WORKS

In this paper, we presented a localization method using 3D point-cloud and road-marker maps. The localization estimation used a particle filtering (PF) algorithm. Normal distribution transform (NDT) scan matching was used for 3D point-cloud map-based localization. In order to incorporate a pose estimated by NDT in a PF algorithm, we determined its pose uncertainty offline in a pre-experiment where different initialization conditions for NDT were performed. Then, we used the resulting NDT offline estimation results to determine the uncertainty (covariance matrix) of the matching, which is dependent on the environmental configuration.

To determine the uncertainty of the NDT result, we compared the proposed method with an approach that uses the Hessian matrix. Comparison results showed that the pre-determined uncertainty well represents the uncertainty of the NDT result compared with the Hessian matrix-based method. In addition, we evaluated the localization accuracy based on the road-marker matching rate, which indicates the relative localization accuracy from the road marker. From the evaluation, we verified that the localization accuracy could be improved by using the proposed method.

In our future work, we aim to determine the uncertainty of the NDT result online. The results of the pre-experiment used to determine the uncertainty of the NDT implied that the convergence performance of NDT depends on the environmental configuration around the vehicle. There are larger errors in open spaces (e.g., country-side rice fields) in which there are no structures (i.e., buildings) around the vehicle compared to typical urban environments. In addition, the uncertainty should be predicted from the current localization result because NDT convergence strongly depends on the

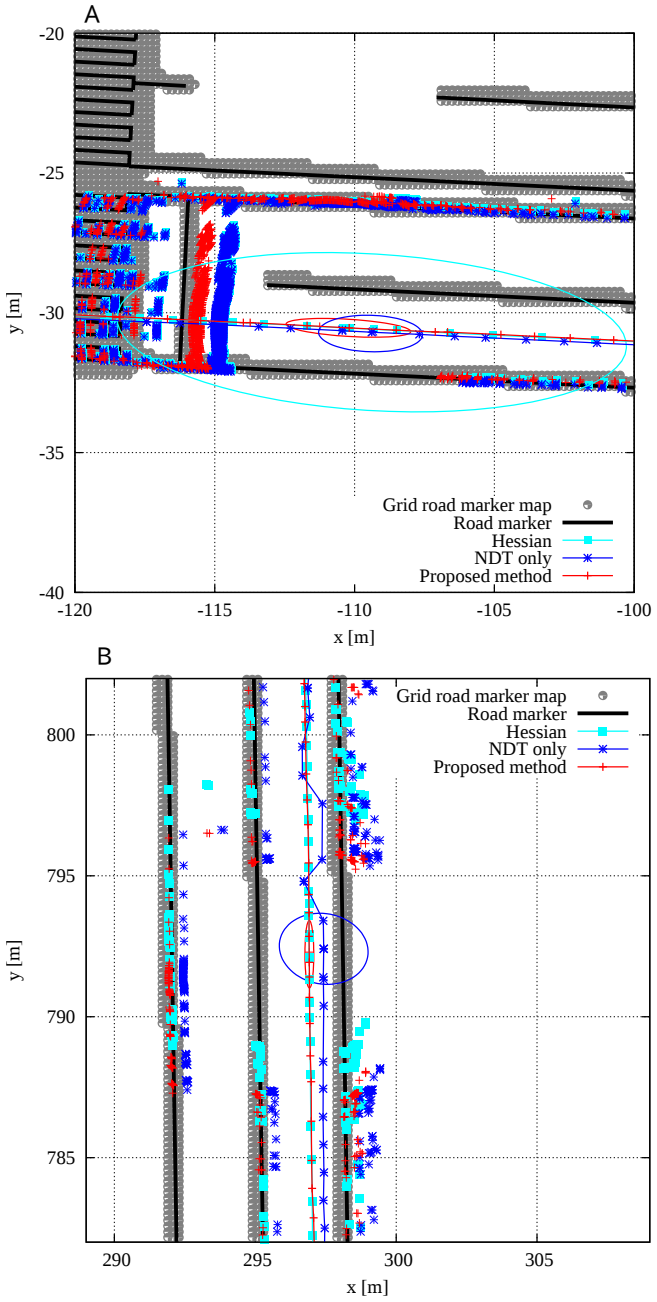

Fig. 13. Estimated trajectories and error ellipses of each method near areas A and B. The points detected as road markers are also depicted in the same color as that of the estimated pose. The estimated pose obtained by NDT only is slightly different from the ground truth because the road marker is not matched. However, the errors may be covered by the uncertainty, which is determined through the pre-experiment. Note that the error ellipse that is computed from the Hessian matrix is drawn in the bottom figure, but it is not shown because the range of the ellipse is very large. As can be seen in both figures, the pre-determined uncertainty well estimated the error of NDT.

initial pose. This means that we should expect the uncertainty to be large when the uncertainty of the initial pose is large. We will consider how it may be achieved by using machine-learning-based methods.

ACKNOWLEDGMENT

This research was supported by the Center of Innovation Program (Nagoya-COI; Mobility Society leading to an Active and Joyful Life for Elderly) from the Japan Science and Technology Agency.

REFERENCES

[1] AISAN TECHNOLOGY Co. Ltd., "MMS by AISAN TECHNOLOGY," http://www.whatmms.com/, accessed on January 6, 2017.
[2] A. Hata *et al.*, "Road marker detection using LIDAR reflective intensity data and its application to vehicle localization," *IEEE International Conference on Intelligent Transportation Systems*, pp. 584-589, 2014.
[3] M. Aldibaja *et al.*, "Improving localization accuracy for autonomous driving in snow-rain environments," *IEEE/SICE International Symposium on System Integration*, pp. 212-217, 2016.
[4] C. Brenner, "Global localization of vehicles using local pole patterns," *in Pattern Recognition. Springer* pp. 61-70, 2009.
[5] B. Qin *et al.*, "Curb-intersection feature based Monte Carlo Localization on urban roads," *IEEE International Conference on Robotics and Automation*, pp. 2640-2646, 2012.
[6] X. Qu *et al.*, "Vehicle localization using mono-camera and geo-referenced traffic signs," *IEEE Intelligent Vehicles Symposium*, 2015.
[7] J. Levinson *et al.*, "Robust vehicle localization in urban environments using probabilistic maps," *IEEE International Conference on Robotics and Automation*, pp. 4372-4378, 2010.
[8] N. Suganuma *et al.*, "Localization for autonomous vehicle on urban roads," *Journal of Advanced Control, Automation and Robotics*, vol. 1, no. 1, pp. 47-53, 2015.
[9] A. Schlichting *et al.*, "Vehicle localization by LIDAR point correlation improved by change detection," *International Archives of the Photogrammetry, Remote Sensing and Spatial Information Sciences*, vol. XLI-B1, pp.703-710, 2016.
[10] P. Biber *et al.*, "The normal distributions transform: A new approach to laser scan matching," *IEEE/RSJ International Conference on Intelligent Robots and Systems*, vol. 3, 2003.
[11] M. Magnusson *et al.*, "Scan registration for autonomous mining vehicles using 3D-NDT," *Journal of Field Robotics*, vol. 24, no. 10, pp. 803-827, 2007.
[12] M. Magnusson *et al.*, "Evaluation of 3D registration reliability and speed - A comparison of ICP and NDT," *IEEE International Conference on Robotics and Automation*, 2009.
[13] F. Dellaert *et al.*, "Monte Carlo localization for mobile robots," *IEEE International Conference on Robotics and Automation*, 1999.
[14] K. Yoneda *et al.*, "Urban road localization by using multiple layer map matching and line segment matching," *IEEE Intelligent Vehicles Symposium*, 2015.
[15] O. Bengtsson *et al.*, "Localization in changing environments - estimation of a covariance matrix for the IDC algorithm," *IEEE/RSJ International Conference on Intelligent Robots and Systems*, 2001.
[16] A. Censi, "An accurate closed-form estimate of ICP's covariance," *IEEE International Conference on Robotics and Automation*, 2007.
[17] E. B. Olson, "Real-time correlative scan matching," *IEEE International Conference on Robotics and Automation*, 2009.
[18] J. Saarinen *et al.*, "Normal distributions transform Monte-Carlo localization (NDT-MCL)," *IEEE/RSJ International Conference on Intelligent Robots and Systems*, pp. 382-389, 2013.
[19] R. Valencia *et al.*, "Localization in highly dynamic environments using dual-timescale NDT-MCL," *IEEE International Conference on Robotics and Automation*, 2014.
[20] E. Takeuchi *et al.*, "A 3-D scan matching using improved 3-D normal distributions transform for mobile robotic mapping," *IEEE/RSJ International Conference on Intelligent Robots and Systems*, pp. 3068-3073, 2006.
[21] F. Moosmann *et al.*, "Velodyne SLAM," *IEEE Intelligent Vehicles Symposium*, pp. 393-398, 2011.
[22] A. Doucet *et al.*, "Sequential Monte Carlo methods in practice," *Springer*, 2001.
[23] K. Kanatani, "Statistical optimization for geometric computation - Theory and practice," *Dover Publications*, 2005.